The Effects of Mesoscale Eddies on the Main Subtropical Thermocline

CARA C. HENNING AND GEOFFREY K. VALLIS

Geophysical Fluid Dynamics Laboratory, Princeton University, Princeton, New Jersey

ABSTRACT

The effects of mesoscale eddies on the main subtropical thermocline are explored using a simply configured wind- and buoyancy-driven primitive equation numerical model in conjunction with transformed Eulerian mean diagnostics and simple scaling ideas and closure schemes. If eddies are suppressed by a modest but nonnegligible horizontal diffusion and vertical diffusion is kept realistically small, the model thermocline exhibits a familiar two-regime structure with an upper, advectively dominated ventilated thermocline and a lower, advective–diffusive internal thermocline, and together these compose the main thermocline. If the horizontal resolution is sufficiently high and the horizontal diffusivity is sufficiently low, then a vigorous mesoscale eddy field emerges. In the mixed layer and upper-mode-water regions, the divergent eddy fluxes are manifestly across isopycnals and so have a diabatic effect. Beneath the mixed layer, the mean structure of the upper (i.e., ventilated) thermocline is still found to be dominated by mean advective terms, except in the ''mode water'' region and close to the western boundary current. The eddies are particularly strong in the mode-water region, and the low-potential-vorticity pool of the noneddying case is partially eroded away as the eddies try to flatten the isopycnals and reduce available potential energy. The intensity of the eddies decays with depth more slowly than does the mean flow, leading to a three-way balance among eddy flux convergence, mean flow advection, and diffusion in the internal thermocline. Eddies subduct water along isopycnals from the surface into the internal thermocline, replenishing its water masses and maintaining its thickness. Just as in the noneddying case, the dynamics of the internal thermocline can be usefully expressed as an advective–diffusive balance, but where advection is now by the residual (eddy-induced plus Eulerian mean) circulation. The eddy-induced advection partially balances the mean upwelling through the base of the thermocline, and this leads to a slightly thicker thermocline than in the noneddying case. The results suggest that as the diffusivity goes to zero, the residual circulation will go to zero but the thickness of the internal thermocline may remain finite, provided eddy activity persists.

1. Introduction

Understanding the structure of the ocean stratification is a fundamental problem in ocean circulation dynamics, and the main thermocline is the single most obvious feature of this stratification. Yet even the simpler problem of understanding the structure of the thermocline of an idealized ocean consisting of a single, isolated basin with a single subtropical and subpolar gyre is not fully understood. The particular geography of the ocean basins and the circulation between them will surely play an important role in modifying the structure revealed by such a simple model. However, the dynamics of the thermocline of an idealized basin will likely transcend such geographical modifications and be relevant to the real ocean, especially for the main Northern Hemisphere basins where the influence of the Southern Ocean on the main thermocline is limited. Certainly, it is unlikely that the dynamics of the thermocline in the real ocean

can be understood without understanding the dynamics of such models.

Consider first an idealized extraequatorial ocean, with wind forcing such as to produce both a subtropical and subpolar gyre, and buoyancy forcing such that the subtropical gyre is warmed and the subpolar gyre cooled, effectively prescribing the surface temperature except in regions of strong western boundary currents. Suppose further that the diapycnal thermal diffusivity is (realistically) small, and that baroclinic instability is (less realistically) suppressed via the use of the planetary geostrophic equations and a small but nonnegligible horizontal diffusivity. In these circumstances Samelson and Vallis (1997, henceforth SV) showed that the main subtropical thermocline has two main dynamical regimes. The upper regime, comprising isopycnals that outcrop in the region of Ekman downwelling (the subtropical gyre), is advectively dominated, forming a ventilated thermocline similar to that appearing in the calculation of Luyten et al. (1983)—a regime that was partly anticipated by Welander (1959), and analyzed further by Huang (1988). The lower thermocline, comprising isopycnals that outcrop in the region of Ekman suction (the subpolar gyre), is characterized by an advective–

Corresponding author address: Geoffrey K. Vallis, Princeton University, AOS Program, Sayre Hall, Princeton, NJ 08544.
E-mail: gkv@princeton.edu

diffusive balance, forming an internal thermocline similar to those suggested by Robinson and Stommel (1959), Stommel and Webster (1963), and Salmon (1990) and analyzed further by Samelson (1999). The main thermocline consists of the ventilated *and* internal thermoclines. In each case, the dominant balance in the thermodynamic equation along with the assumptions of thermal wind and continuity give scaling predictions for how the average depth of the ventilated thermocline and thickness of the internal thermocline will vary with model parameters such as the wind stress and diffusivity, and SV verified these predictions in their model.

The primary shortcoming of the SV model is its lack of mesoscale eddies—in fact, such eddies were purposely omitted from that model. However, the eddy kinetic energy of the ocean is at least an order of magnitude larger than the mean kinetic energy, and it has long been recognized that eddy effects may be important in the oceanic general circulation. Rhines and Young (1982) suggested that eddies would be an effective way of producing subsurface motion and of homogenizing potential vorticity in closed gyres, and Cox (1985), using a primitive equation numerical model, investigated the effect of eddies on the ventilated thermocline (although his integration length was too short to draw definitive conclusions). Vallis (2000) and, more explicitly, Marshall et al. (2002) wondered whether mesoscale eddies might indeed be an important factor in determining the stratification itself, rather than being a perturbation about it. Since then Karsten et al. (2002) and Radko and Marshall (2003) have found eddies to be important in very idealized simulations.

Our goal in this paper is to explore the effects of mesoscale eddies on the ocean stratification using a primitive equation numerical model, configured in an idealized but oceanographically relevant domain. Our focus is on the main subtropical thermocline (in a subsequent paper we will report on the effects of a simple circumpolar channel), and we will run at both noneddying and eddy-permitting resolutions. In particular, we wish to answer the following questions:

1) How does the mean stratification depth and thickness differ in the two cases, and can this result be captured by simple scaling theories?
2) How do the details of the stratification in the eddy-permitting case differ from those in the case without eddies?

Answering these involves both a qualitative look at the differences between individual isopycnals and a more detailed evaluation of the overall balance of terms in the thermodynamic equation. We perform a number of experiments in which we change model parameters (e.g., wind strength, diffusivity) and investigate if and how the overall structure of the thermocline changes as a consequence. The numerical experiments are performed in a relatively small domain (somewhat smaller than the North Atlantic basin), but are all integrated for a long period (>100 yr at eddying resolution, after a lower-resolution spinup of thousands of years) in order to ensure that their thermodynamic structure properly equilibrates. Section 2 discusses the experimental setup, and this is followed by a rather crude scaling analysis (section 3) in order to grasp the orders of magnitude involved in the eddy effects. Section 4 describes the changes in the details and overall character of the stratification, and section 5 describes the effects of changing model parameters. This is followed by a general summary and discussion.

2. Numerical model and experimental design

Equations of motion

We use a primitive equation ocean model, the Geophysical Fluid Dynamics Laboratory (GFDL) Modular Ocean Model (MOM)-3 (Pacanowski and Griffies 1999) in an enclosed, flat-bottomed, rectangular basin 23° longitude in width and stretching from 12° to 48°S.[1] The equations of motion solved by the model are

$$\frac{Du}{Dt} - fv = -\frac{1}{\rho_o}\frac{\partial p}{\partial x}, \tag{1a}$$

$$\frac{Dv}{Dt} + fu = -\frac{1}{\rho_o}\frac{\partial p}{\partial y}, \tag{1b}$$

$$\frac{\partial p}{\partial z} = -\rho g, \tag{1c}$$

$$\frac{D\theta}{Dt} = \kappa_v \theta_{zz}, \quad \text{and} \tag{1d}$$

$$\nabla \cdot \mathbf{v} = 0, \tag{1e}$$

as well as a linear equation of state connecting density with potential temperature. (The viscous and forcing terms in the momentum equations and the experiment-dependent subgrid parameterizations are omitted.) These are the usual hydrostatic, Boussinesq equations with no salinity. Thus, p is the pressure; θ is potential temperature; $\rho = \rho_0 + \rho'$ is the density; u, v, and w are the usual horizontal and vertical velocity components; and κ_v is the vertical diffusivity. If we write $p = p_0(z) + \rho_0\phi$, where p_0 is in hydrostatic balance with ρ_0, then the hydrostatic relation becomes

$$\frac{\partial \phi}{\partial z} = b, \tag{2}$$

where $b = -\rho'g/\rho_0$ is the buoyancy. For later theoretical and scaling work we note that the thermodynamic equation may be written in terms of buoyancy as

---

[1] The experiments are carried out in a nominal Southern Hemispheric domain to provide comparison with later work in which we add a circumpolar channel near the southern boundary.
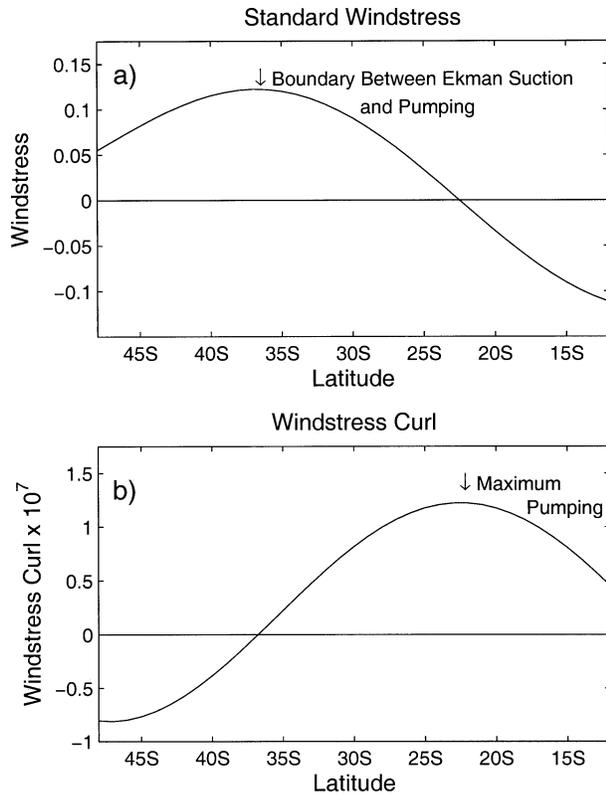
FIG. 1. (top) The standard wind stress (N m^{-2}) and (bottom) the curl of the wind stress (N m^{-3}) used in the base case. The wind stress curl has a maximum near 23°S.

TABLE 1. A summary of the experiments run with varying diffusivity and wind. "Standard" refers to the wind profile given in Fig. 1.

	κ_v (m^2 s^{-1})	Wind stress	Length of eddy simulation (yr)
Base case	2×10^{-5}	Standard	150
Wind $\times$ 0.75	2×10^{-5}	Standard $\times$ 0.75	150
Wind $\times$ 1.25	2×10^{-5}	Standard $\times$ 1.25	105
Wind $\times$ 1.5	2×10^{-5}	Standard $\times$ 1.5	140
Diff $\times$ 0.5	1×10^{-5}	Standard	150
Diff $\times$ 1.5	3×10^{-5}	Standard	100
Diff $\times$ 2	4×10^{-5}	Standard	150

$$\frac{Db}{Dt} = \kappa_v b_{zz}. \tag{3}$$

The model is mechanically forced using an idealized "two gyre" zonal wind stress, which is a function of latitude only. The wind stress curl, shown in Fig. 1, has a maximum near 24°S and it changes sign at 37°S, giving a rather larger subtropical gyre than subpolar gyre. The only active tracer in the model is temperature and the model is thermodynamically forced by relaxing the uppermost grid value of temperature to a prescribed value that falls linearly with latitude. Specifically, we use a restoring coefficient of 50 W m^{-2} (°C)$^{-1}$, giving a restoring time scale of 10 days with an the upper-layer thickness of 10 m. A simple convective adjustment scheme and a bottom drag with a constant, dimensionless drag coefficient of $c_d = 5 \times 10^{-3}$ are also employed, where the bottom stress is given by $\rho_0 c_d |u| \mathbf{u}$, where $\mathbf{u}$ is the horizontal velocity and $|u|$ is its magnitude.

The simulations were carried out in several stages. First, integrations were completed at relatively coarse resolution, with a grid size of approximately 2°. This scale is too coarse to resolve the radius of deformation, and these runs represent the noneddying cases. A uniform Laplacian horizontal diffusion of potential temperature [$\kappa_h(\theta_{xx} + \theta_{yy})$] was used, with a diffusivity of 50 m^2 s^{-1}, which is the smallest value that maintained

numerical stability. This diffusivity is two orders of magnitude smaller than those typically used to capture eddy mixing in low-resolution models, implying the cases are as close in interpretation to "noneddying" as possible. Also, away from the western boundary current, the horizontal diffusion resulting from this small diffusivity is negligible in comparison with the vertical diffusion, implying the Veronis effect (Veronis 1975) is small and the cross-isopycnal mixing induced by the subgrid-scale parameterizations is substantially captured by the vertical diffusion. The horizontal viscosity is also Laplacian and is adjusted so that the Munk western boundary layer is marginally resolved (5×10^4 m^2 s^{-1}).

The vertical resolution is kept as high as computational resources allow, with the same vertical resolution used in all experiments. The resolution is 10 m at the surface, stretched to 30 m at 500-m depth, and increased to 890 m at 4000-m depth (the domain bottom), with a total of 50 vertical layers. The model is first run as a base case with the given winds and with a uniform Laplacian vertical diffusivity of $\kappa_v = 2 \times 10^{-5}$ m^2 s^{-1} and Laplacian viscosity of 1×10^{-4} m^2 s^{-1}. In addition, four other cases are run with varying winds and vertical diffusion parameters, as summarized in Table 1. These low-resolution cases are run at little expense; therefore, we started them from a uniform potential temperature and integrated them for 20 000–30 000 yr to reach a fully equilibrated state, and the thermocline depth and thickness are found to follow the SV scalings (not shown).

The end states of these integrations then become the initial condition for the integrations with much higher horizontal resolution, which develop vigorous mesoscale eddies. Thus, the final state at a 2° resolution was interpolated onto a 1/6° grid and the integration continued.[2] The vertical grid, diffusivity, and viscosity were left unchanged. However, the horizontal viscosity parameterization was changed to a biharmonic scheme and, following a suggestion in Griffies et al. (2000), the viscosity was set at an intermediate value of 1×10^{11} m^4 s^{-1}. This value is large enough to minimize indirect

---

[2] The resolution refers to the longitudinal resolution. The latitudinal resolution varies with latitude to keep the grid nearly square and is always finer than this resolution in terms of degrees.

dispersion errors in the tracer field due to the advection scheme, but not so large as to overly damp the eddy kinetic energy. Last, the horizontal diffusion scheme in the thermodynamic equation was eliminated in favor of the Gent–McWilliams (GM) scheme (Gent et al. 1995) to eliminate tracer variance at the grid scale. Usually this scheme is used to mix thickness along isopycnals and thus to mimic eddy effects in noneddy resolving models; however, we use it merely as a device to adiabatically eliminate small-scale noise. Thus, the GM coefficient is $\kappa_{GM} = 5 \times 10^{-1}$ m^2 s^{-1}, 3–4 orders of magnitude smaller than values typically chosen to simulate eddy effects (see, e.g., Nakamura and Chao 2000; Kamenovich et al. 2000). Again, the resulting magnitude is small compared to the vertical diffusion. Because the vertical diffusivity is kept constant between the low-resolution and eddy-permitting runs, then for identical stratification profiles, both cases will have substantially the same cross-isopycnal subgrid-scale diffusion (although the eddy case may have an additional eddy-induced cross-isopycnal mixing).

The high-resolution experiments were typically run for about 120–150 yr, which was found sufficient to equilibrate the thermocline. Much of our analysis focuses on the subtropical gyre just east of the western boundary current, and our primary "diagnostics region" extends from about 6° to 8° east of the western boundary and from 25° to 17°S. This is an eddy-rich region where the source of available potential energy from the Ekman pumping is large, but it is not within the western boundary layer.

3. Scaling analysis

Equations of motion

Dividing the buoyancy equation into time mean and eddying component in the usual way gives the time-averaged thermodynamic equation,

$$\overline{u}\overline{b}_x + \overline{v}\overline{b}_y + \overline{w}\overline{b}_z$$
$$= -(\overline{u'b'})_x - (\overline{v'b'})_y - (\overline{w'b'})_z + \kappa_v \overline{b}_{zz}, \quad (4)$$

where $(\overline{})$ indicates a quantity averaged in time and $()'$ indicates the deviation of that quantity from the time average. The importance of mesoscale eddies to this balance may be roughly estimated by comparing the sizes of the two terms

$$\nabla \cdot \overline{u'b'} \quad \text{and} \quad \nabla \cdot (\overline{u}\overline{b}). \quad (5)$$

If we take $b' \sim \delta \mathbf{x} \cdot \nabla \overline{b} \sim L_e \Delta b / L$, where L_e is an eddy scale and Δb and L refer to the scales of mean quantities, then the ratio of the magnitude of the eddy terms to the mean advection is

$$\mu_{VT} \sim \frac{U_e L_e}{UL}, \quad (6)$$

which is the inverse of an eddy Peclet number Pe =

UL/U_eL_e. If μ_{VT} is $O(1)$, then the eddies will participate in the buoyancy equation balance.

To understand how the parameter μ might vary in different oceanic regimes, we can try to estimate its magnitude a priori. Suppose that the eddy scale is proportional to the deformation radius, $L_{def} \sim ND/f$, where $N \sim (\Delta b/D)^{1/2}$ is the buoyancy frequency and D is a depth scale. If we take D to be the depth of the thermocline given by the classical ventilated thermocline scaling,

$$D_a \sim W_E^{1/2}\left(\frac{fL^2}{\Delta b}\right)^{1/2}, \quad (7)$$

we obtain an a priori estimate of the deformation scale,

$$L_d \sim \left(\frac{D\Delta b}{f^2}\right)^{1/2} \approx \left(\frac{W_E \Delta b L^2}{f^3}\right)^{1/4}. \quad (8)$$

Using $\Delta b \sim g\alpha\Delta T$ and $g \approx 10$ m^2/s, $\alpha \approx 10^{-4}$ K^{-1}, $L \approx 10^6$ m, $\Delta T \approx 20$ K, and $D \approx 10^3$ m, then $L_d \approx 50$ km and $L_d/L \approx 0.05$. Observations suggest a similar value for the value of the deformation radius in the midlatitude ocean. Chelton et al. (1998), for example, find that the first deformation radius varies between about 20 and 100 km in midlatitudes, with values of about 50 km being typical in the subtropical gyres. Eddies themselves tend to be rather larger than this, probably reflecting both a weak inverse cascade and also the tendency of the length scale of maximum instability to be larger than the deformation radius. Given this, we have

$$\mu = \frac{U_e L_d}{UL} \sim 0.05\frac{U_e}{U}. \quad (9)$$

Observations (and our simulations, described in later sections) indicate that the eddy kinetic energy is much larger than the mean kinetic energy; in the main gyre, the eddy energy can be 20 times the mean energy (Wyrtki et al. 1976; Stammer 1997), suggesting that the eddy velocity is 4 or 5 times the mean velocity in these cases. Supposing U_e/U to be $O(1)$–$O(10)$ then μ varies between 0.05 and 0.5, indicating that although eddies will certainly have some effect on the upper thermocline, they need not completely overwhelm the structure that would be apparent in their absence.

Other scalings are possible. If we choose the eddy length scale to be the size of the baroclinic zone, then $\mu = O(1)$ and eddy effects are obviously important (assuming $U_e \gtrsim U$), but this likely overestimates their importance. Geostrophic turbulence theory suggests that eddies might, by way of nonlinear effects, grow until their size is limited by Rossby wave radiation (Rhines 1975; Vallis and Maltrud 1993). In that case

$$L_e \sim \sqrt{\frac{U_e}{\beta}} \sim \sqrt{\frac{\Delta b D a}{f^2 L}}, \quad (10)$$

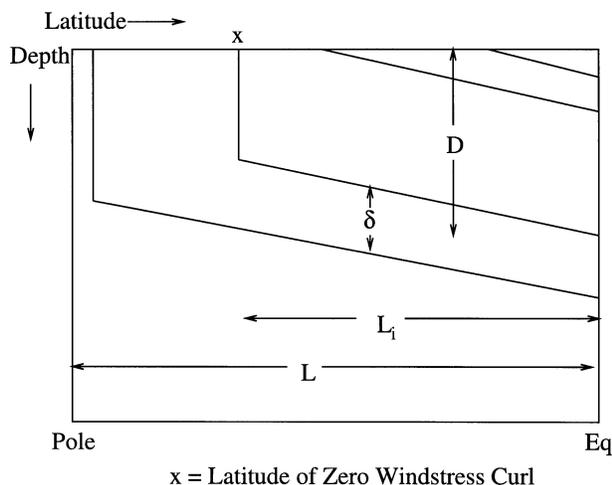where we have used $\beta \sim f/a$ where a is the radius of

Fig. 2. Relevant length scales for the thermocline problem, where D is the depth of the thermocline, L is the length of the domain, δ is the thickness of the internal thermocline, and L_i is the internal horizontal length scale in the internal thermocline.

the earth and $U_e \sim U$, where we have assumed U is given by the thermal wind relation. Using (7) for D, then

$$L_e \sim \left(\frac{W_E \Delta b L^2}{f^3}\right)^{1/4} \left(\frac{a}{L}\right)^{1/2}. \qquad (11)$$

In comparison with (8), using the Rhines scale adds a factor of $(a/L)^{1/2}$ to the prediction for μ. This ratio is also $O(1)$ or somewhat larger, so that μ may approach unity.

Notwithstanding the uncertainty of the scaling theory, we might expect eddy effects to be *more* important in the lower thermocline than in the ventilated thermocline, at least away from the surface. This may seem counterintuitive since eddies tend to be strongest near the surface; however, over their life cycle, eddies will tend to cascade energy to graver vertical scales (Smith and Vallis 2002), distributing some eddy energy over the entire depth of the thermocline. The intensity of the mean flow, however, falls off fairly rapidly with depth so that the ratio U_e/U may actually *increase* with depth. In the classical (noneddying) model the balance in the lower subtropical thermocline is between mean flow and diffusion; the presence of mesoscale eddies suggests the possibility of a subsurface balance involving eddy, mean, and diffusive terms. Below the mixed layer, any eddy effects are likely to be predominantly adiabatic— that is, even though they may certainly affect the thermocline structure, they do so without directly changing the census of water masses. This is not the case at the surface, where we expect (and as we shall see) eddies can have an explicitly diabatic effect, because of the direct contact with the overlying atmosphere. This is because in the ocean interior the explicitly diabatic term, (κb_{zz}), is small and effective only on a time scale much longer than an eddy turnover time, whereas at the sur-
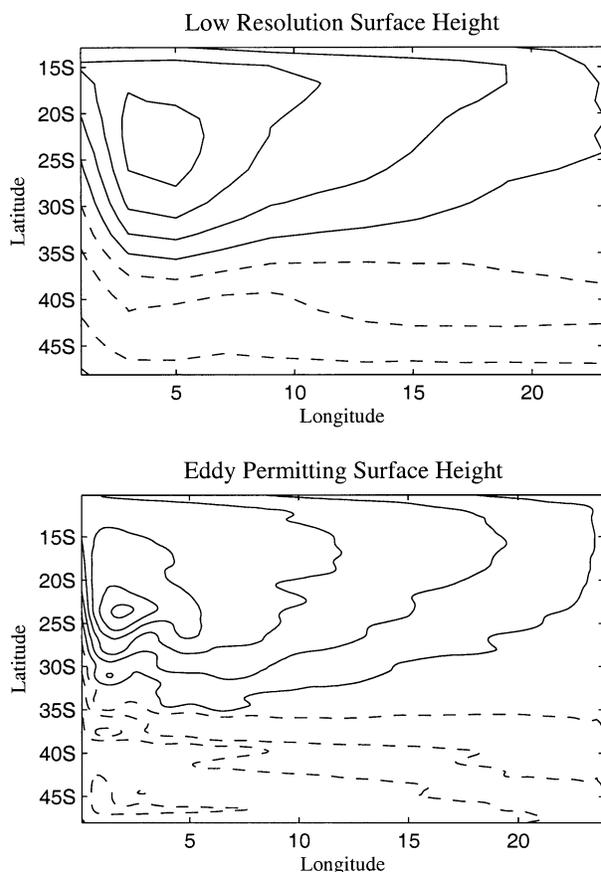

Fig. 3. The time-averaged surface height for the (top) low-resolution and (bottom) eddy-permitting cases. The solid lines show positive heights, and the dashed lines show negative heights. The contour interval in both panels is 10 cm.

face the exchange of sensible heat with the atmosphere occurs on time scales comparable to an eddy time, and water mass properties are not preserved on an advective time scale.

Although such general properties as the above can be inferred by analytic and intuitive reasoning, to gain more quantitative results we turn to numerical simulation.

4. Eddying and noneddying simulations

a. Qualitative overview

Figure 2 illustrates the relevant scales of motion, and Fig. 3 shows the mean surface height for the low-resolution (upper) and eddy-permitting (lower) cases in the control case (see Table 1). Both steady and eddying cases display the two-gyre structure imposed by the wind, with the division between the gyres near the latitude of zero wind stress curl at 35°S. Both cases also have a strong western boundary current, and this current separates from the coast and penetrates to about 5°E. In the eddying case, the western boundary region is nar-
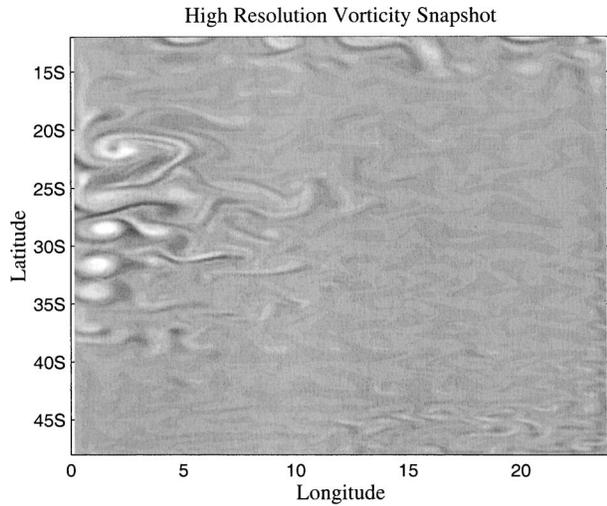
High Resolution Vorticity Snapshot

FIG. 4. A snapshot of the surface vorticity field for the high-resolution case. The field shows small-scale eddy structures in the western boundary region, with the eddies tapering off away from this region. The contours in the above figure range from -4×10^{-5} to 4×10^{-5} s^{-1}.
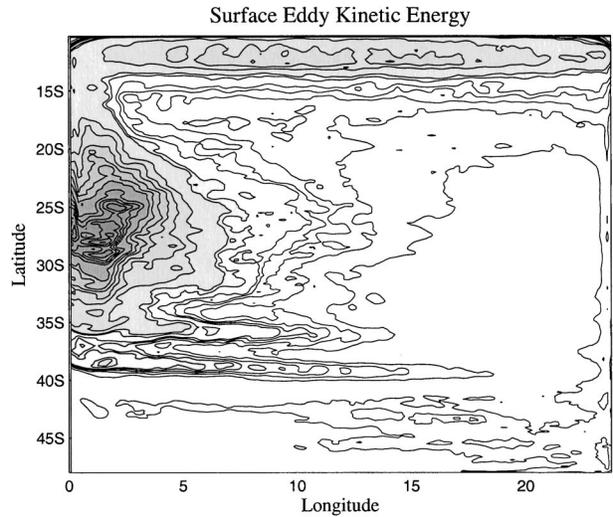
Surface Eddy Kinetic Energy

FIG. 5. The time-averaged surface eddy kinetic energy for the eddy-permitting base case. The eddy kinetic energy is largest in the western boundary current and near the northern domain boundary. In the figure, the range of values is 0–0.3 m^2 s^{-2}, with a contour interval of 0.05 m^2 s^{-2}.

rower and stronger, although the penetration into the interior is similar.

Figure 4 shows a snapshot of the surface vorticity for the high-resolution base case. Disturbances identifiable as mesoscale eddies are present, typically forming in the western boundary region where the velocity shears are greatest and near the latitude of greatest downwelling (25°S). Clearly distinguishable eddies are less visible polewards of 35°S, where the wind stress curl changes sign and there is no longer an input of available potential energy from the Ekman pumping. The eddies typically have a horizontal scale of about 100–200 km, which is somewhat larger than the radius of deformation (which is about 50 km) and which is significantly larger than the grid size, which is about 15 km. However, they are still much smaller than the domain size.

Figure 5 shows the eddy kinetic energy near the surface for the eddying base case. Again, the eddy energy is clearly largest in the western boundary region, with smaller values spreading outward into the gyre. There are also moderate amounts of eddy kinetic energy at the northern boundary of the domain; this energy is produced by eddies that form as a result of the horizontal velocity shear caused by the wall (these latitudes are excluded from the analysis). The ratio of the eddy to mean kinetic energy at the surface varies from little larger than unity (in the eastern gyre) to about 15 (just east of the western boundary current, where much of our analysis is carried out) with a mean value of 7. This is comparable to, if a little smaller than, the real ocean gyre, where the ratio of the kinetic energies has been variously reported as approximately 25 by Wyrtki et al. (1976), 16 by Stammer (1997), and having gyre average of 5.6 (Richardson 1983).

Figure 6 shows a depth–latitude potential temperature section averaged over the gyre region for the low resolution (solid) and eddy permitting (dashed) cases. In general, the thermocline stratification is confined to the upper 400 m. This is shallower than in the real ocean since the latitudinal extent (and thus total range of temperatures) has been limited in this study for computational reasons, although the gradient is roughly consistent with that in the ocean. The model thermocline can usefully be separated into various regions: (i) the ventilated thermocline, which is subject to Ekman pumping and encompasses all isotherms that outcrop between the northern boundary and approximately 27°S; (ii) the

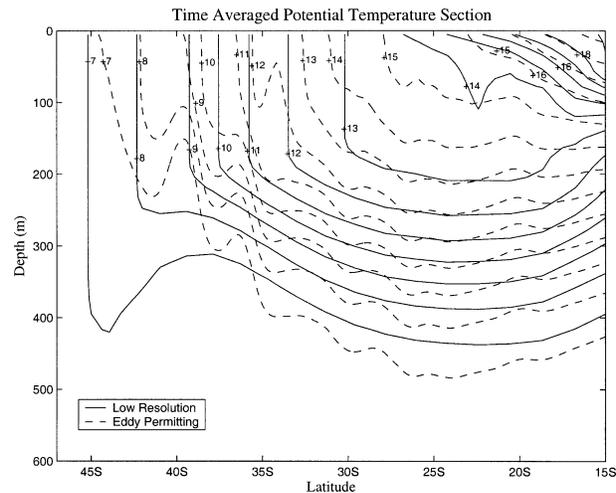Time Averaged Potential Temperature Section

FIG. 6. The time-averaged temperature section for the low-resolution (solid) and eddy-permitting (dashed) cases (°C). The temperature has been averaged from 6° to 8°E.
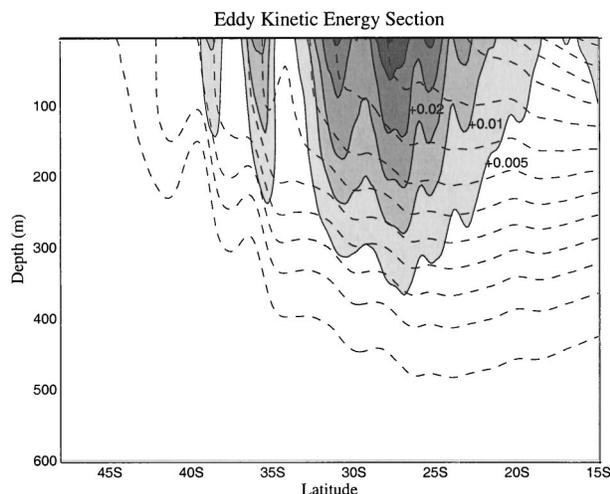
FIG. 7. The eddy kinetic energy averaged from 6° to 8°E, plotted with a contour interval of 5×10^{-3} m^2 s^{-2}. Also shown with dashed contours are the time-averaged isopycnals. The eddy kinetic energy is largest in the former mode water region near 25°–30°S. This is the region that sees the largest change when eddies are added.

mode water region, which is also subject to Ekman pumping but has regions of isothermal water in the low-resolution case and encompasses all isotherms that outcrop between 27° and 35°S; and (iii), the internal thermocline, which encompasses all isotherms that outcrop from 35°S to the southern boundary, in regions of Ekman suction (i.e., the subpolar gyre). We next examine how the eddies affect both the location of individual isotherms (the details of the stratification) and the overall regional gradient (the mean stratification) in each of these regions.

b. Ventilated thermocline and mode water regions

1) THE DEPTH OF THE VENTILATED THERMOCLINE

In the uppermost region of the ventilated thermocline, changes in stratification due to eddies are modest (Fig. 6). However, the isotherms that outcrop in the region of most vigorous eddy activity change position more noticeably. The 13°, 14°, and 15° isotherms deepen and outcrop at latitudes poleward of their low resolution counterparts. Figure 7 shows the eddy kinetic energy section, averaged from latitudes 6 to 8. Indeed, the eddies are strongest in the mode water region, where the changes in the local isotherms are most noticeable. In particular, the warm pool of the mode water region has diminished and the separation between ventilated and internal thermocline is less apparent. The change in the local isotherms is also apparent in profiles of the stratification. Figure 8 shows time-averaged profiles of the vertical temperature gradient for both the low-resolution and eddy-permitting cases. (The profile is also spatially averaged within the diagnostics region.) The entire profile has been smeared out by the eddies, so that the local
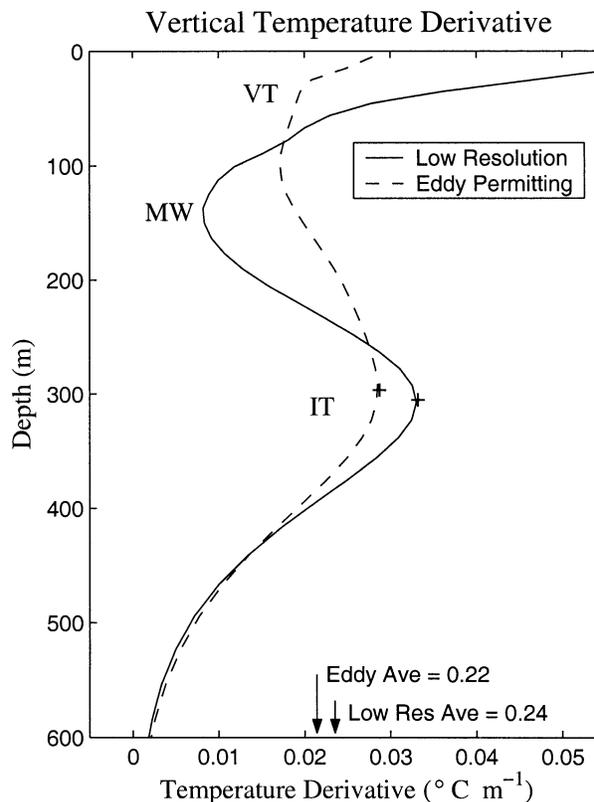

FIG. 8. The time-averaged vertical temperature derivative profile for the low-resolution (solid) and eddying (dashed) cases. The temperature has been averaged from 6° to 8°E and from 17° to 25°S. The ventilated thermocline is indicated by VT, the low-resolution mode water region by MW, and the internal thermocline by IT. The plus signs indicate the depth of the ventilated thermocline, evaluated as the depth of the maximum temperature gradient.

slope has changed and the vertical temperature gradient is more uniform through the column.

The eddies appear to play a large role in setting the surface outcrops and local slope in the mode water region. However, this does not ensure they are affecting the overall mean slope of the ventilated thermocline. In Fig. 8, the average temperature gradient in the Ekman pumping region (listed at the bottom of the figure and averaged from the surface to the depth of the subsurface maximum) is nearly the same in the two cases, with the eddying case gradient only slightly shallower. Accordingly, the depth of the ventilated thermocline, defined by the depth of the subsurface maximum in the temperature gradient and indicated by the + in the figure, remains nearly unchanged. Thus, we find support that the eddies are affecting the individual isotherms in the ventilated thermocline, but the eddies do not seem to constrain the average gradient (or slope) in this region. The scaling for this depth is still likely set by the Ekman pumping and a mean balance in the buoyancy equation, with little contribution from the eddies.

Analysis of the terms in the buoyancy equation shows that, indeed, the eddy terms have a small overall effect
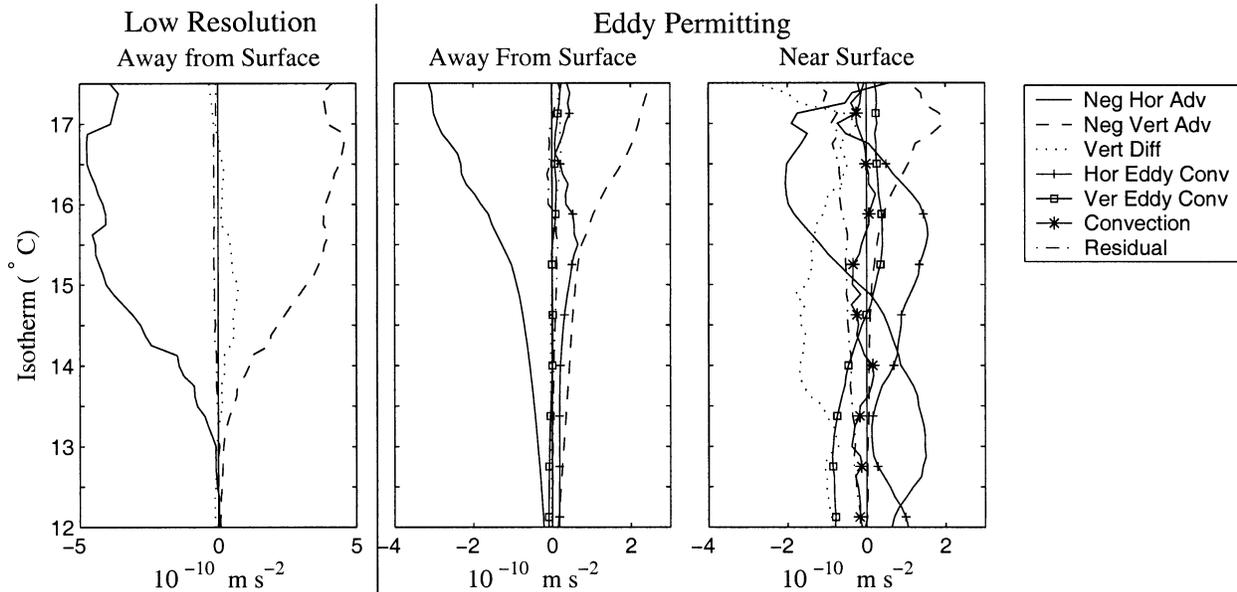
Ventilated Thermocline Buoyancy Terms

FIG. 9. The buoyancy equation terms for the ventilated thermocline. The terms are plotted for (left) the low-resolution case away from the surface, (center) the eddy-permitting case away from the surface, and (right) the eddy-permitting case near the surface. The terms have been averaged along constant isopycnals over the diagnostics region equatorward of 25°S. The terms are negative horizontal advection, $-\overline{ub}_x - \overline{vb}_y$; negative vertical advection, $-\overline{wb}_z$; vertical diffusion, $\kappa_v \overline{b}_{zz}$; horizontal eddy convergence, $-(\overline{u'b'})_x - (\overline{v'b'})_y$; vertical eddy convergence, $-(\overline{w'b'})_z$; and convection, the change in the buoyancy tendency due to the convective adjustment scheme. The horizontal diffusion term, $\kappa_h(\overline{b}_{xx} + \overline{b}_{yy})$, is not included because it is too small to discern on the figure.

on the dominant balance in the ventilated thermocline. Figure 9 shows the buoyancy equation terms for the low-resolution case away from the surface (left), the eddy-permitting case away from the surface (center), and the eddy-permitting case near the surface (right) for the ventilated thermocline. The various terms are time- and spatially averaged in the diagnostics region, with the spatial average performed along isopycnal surfaces. The surface region represents the mixed layer and is identified as grid boxes where the change in temperature due to convection lies above a threshold value. The rest of the water column constitutes the "away from the surface" region. Beneath the surface, the upper thermocline dominant balance is between the mean advection terms in both the low-resolution and eddying cases. Away from mode water regions, the horizontal eddy flux convergence is much smaller than the mean advection terms, and the vertical eddy flux convergence is close to zero. Along isotherms 12–16.5, which is through the mode-water region, the eddy flux convergence is proportionately larger and eddies do participate in the thermodynamic balance.

In the model ventilated thermocline, we find that $U_e/U \approx 3$ and $L_e/L \approx 1/15$. The ratio of the length scales is found by Fourier analyzing the surface kinetic energy and identifying the maximum energy containing scale as the location of the peak of the spectrum (not shown). Thus, the ratio of the eddy and mean terms in the ventilated thermocline is

$$\mu_{VT} = \frac{U_e L_e}{UL} \approx 0.2. \tag{12}$$

An explicit average of the buoyancy equation terms along the isotherms in the ventilated thermocline gives a similar value for this ratio, so that the overall contribution of the eddy terms is small, though not wholly negligible. The eddies have affected the placement of individual isotherms in accordance with creating a more uniform slope, but they have not overwhelmed the dominant balance found in the low-resolution buoyancy equation.

The homogenization of slope in the (former) mode water region is consistent with a reduction in the available potential energy (APE) of the system. The mean volume averaged available potential energy is defined by

$$\text{APE} = \frac{1}{V} \int \frac{(\overline{\rho} - \tilde{\rho})^2}{d\tilde{\rho}/dz} \, dV, \tag{13}$$

where $\overline{\rho}$ is the time mean density field and V is the volume of the domain (Oort et al. 1989). Here, $\tilde{\rho}$ is the time-averaged density averaged at constant height over the domain,

$$\tilde{\rho} = \frac{1}{L_x L_y} \iint \overline{\rho} \, dx \, dy, \tag{14}$$

where L_x and L_y are the lengths of the domain in the

longitudinal and latitudinal directions. In our model, calculating the APE by integrating over the domain gives

$$\text{low-resolution APE} \approx 1320 \text{ J m}^{-3} \quad \text{and}$$

$$\text{eddy-permitting APE} \approx 1170 \text{ J m}^{-3}. \quad (15)$$

To approximately quantify the APE within the ventilated thermocline, we take the integrand in (13) as an APE density and compute this integral over the volume within the 11° isotherm, near the base of the ventilated thermocline. However, $\tilde{\rho}$ remains the average at constant depth over the whole domain. We also exclude the western and northern boundary regions from the integral to focus on the gyre portion of the thermocline. This computation yields

$$\text{low-resolution APE} \approx 648 \text{ J m}^{-3} \quad \text{and}$$

$$\text{eddy-permitting APE} \approx 442 \text{ J m}^{-3}. \quad (16)$$

The simulation with eddies has a lower value of available potential energy. In the low-resolution case, the mode water represents a storage of APE, since a comparatively light water mass exists at depth and forms a sharp front with the heavier water at its poleward edge (identified as the steep 13° isotherm in Fig. 6). When eddies are added, the 13° isotherm outcrop is pushed poleward, the slope decreases, and the mode water is replaced with comparatively less dense water, all consistent with a release of the stored APE and a lower final APE state.

2) SURFACE PROCESSES

The fact that the eddy-permitting isotherms outcrop poleward from their low-resolution counterparts (Fig. 6) suggests the eddies may be playing an important role at the surface. Figure 10 shows the divergent part of the eddy buoyancy flux vectors and the isopycnal contours at the surface, where any contribution from the vertical fluxes has been excluded. In this plot, the western boundary region is excluded. The eddy fluxes are largely directed across the mean isopycnals in the eddy-rich portions of the subtropical gyre (between longitudes 8 and 12 and equatorward of 35°S), suggesting the eddies have a diabatic effect at the surface.

The right panel of Fig. 9 shows the buoyancy equation terms averaged along the ventilated thermocline isotherms near the surface, where the isotherms tend to be steeply sloping and convection is nonzero. Surface restoring is implemented via a vertical diffusion term, so the large negative diffusion in the figure represents the large removal of heat at the surface. Aside from the region around isotherms 13–13.5, the horizontal eddy flux convergence term mixes heat poleward across isotherms and participates in the first-order balance in the buoyancy equation. Though the eddies are not playing a large role in setting the slope of the isotherms within the ventilated thermocline, they are playing a dominant
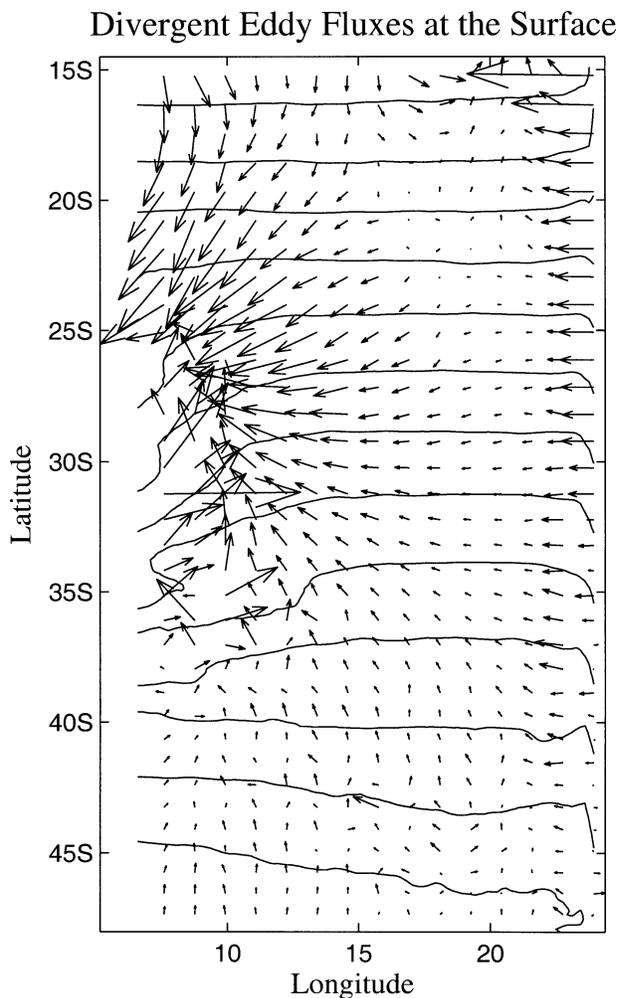

FIG. 10. The divergent part of the eddy buoyancy flux vectors at the surface. The western boundary region is excluded from the figure. This plot excludes any contribution from the vertical fluxes.

role in setting the outcrop latitudes, implying they may affect the subduction of mass from the mixed layer into the thermocline.

To determine the effect of the eddy surface processes on the structure of the thermocline, we ran the low-resolution model with the same parameters as previously described, but we restored the surface temperature to that in the eddy permitting case using a very short restoring time scale (so that the surface temperatures are essentially prescribed to be those in the eddying case). The result captures the low-resolution response to the eddy-determined surface outcrops. Figure 11 shows the temperature section for the original low-resolution case (solid), the eddy-permitting case (dashed), and the low-resolution case restored to the eddy-permitting surface temperatures (dotted, referred to as low-resolution eddy-restored case below). This plot can be compared with Fig. 6, although the contour interval has been increased to 2°C. In this case, the position of the 14°C isotherm
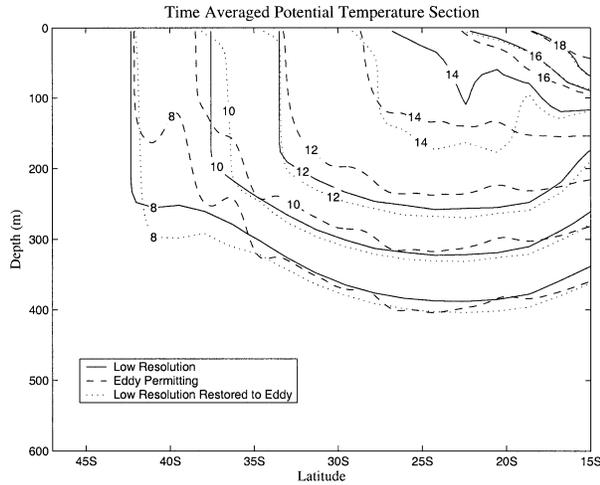
Time Averaged Potential Temperature Section

FIG. 11. The time-averaged temperature section, similar to Fig. 6. However, the dotted line shows the low-resolution case restored to the eddy-permitting case temperature field at the surface. The contour interval is 2°C.

of the low-resolution eddy-restored case is more similar to the eddy-permitting case than the low-resolution case. The altered surface restoring diminishes the mode water in the low-resolution case, implying the surface eddy mixing and resulting change in subduction rates into the main thermocline are largely responsible for the changes seen in the ventilated thermocline structure. We will return to this point in section 5a.

c. The internal thermocline

The internal thermocline is the lower portion of the thermocline containing isotherms that do not outcrop in the region of Ekman downwelling. In noneddying models this is a diffusive transition zone connecting the base of the ventilated thermocline to the abyss, and the diapycnal diffusion is of first order importance no matter how small the diffusivity. We now explore how this structure changes in the presence of mesoscale eddies.

THE THICKNESS OF THE INTERNAL THERMOCLINE

As seen in Figs. 6 and 8, the inclusion of this eddy flux causes the internal thermocline to thicken. The thickness is calculated as the width of the lower half-maximum of the temperature gradient profile. In our control integration, the internal thermocline thickness is 110 m for the low-resolution case and 140 m for the eddying case. Although small, this increase is robust and found in all our integrations.

Figure 12 shows the buoyancy equation terms averaged along the internal thermocline isotherms. In the eddying case, the horizontal eddy flux convergence is as large as the diffusion term, and together they balance the mean vertical advection. To estimate the contribution of the eddies to the buoyancy equation, we find that the ratio of the eddy to mean terms averaged over the internal thermocline isotherms has increased to $\mu_{IT} \approx 0.8$. This is larger than the corresponding ratio in the ventilated thermocline. As noted previously, this is because
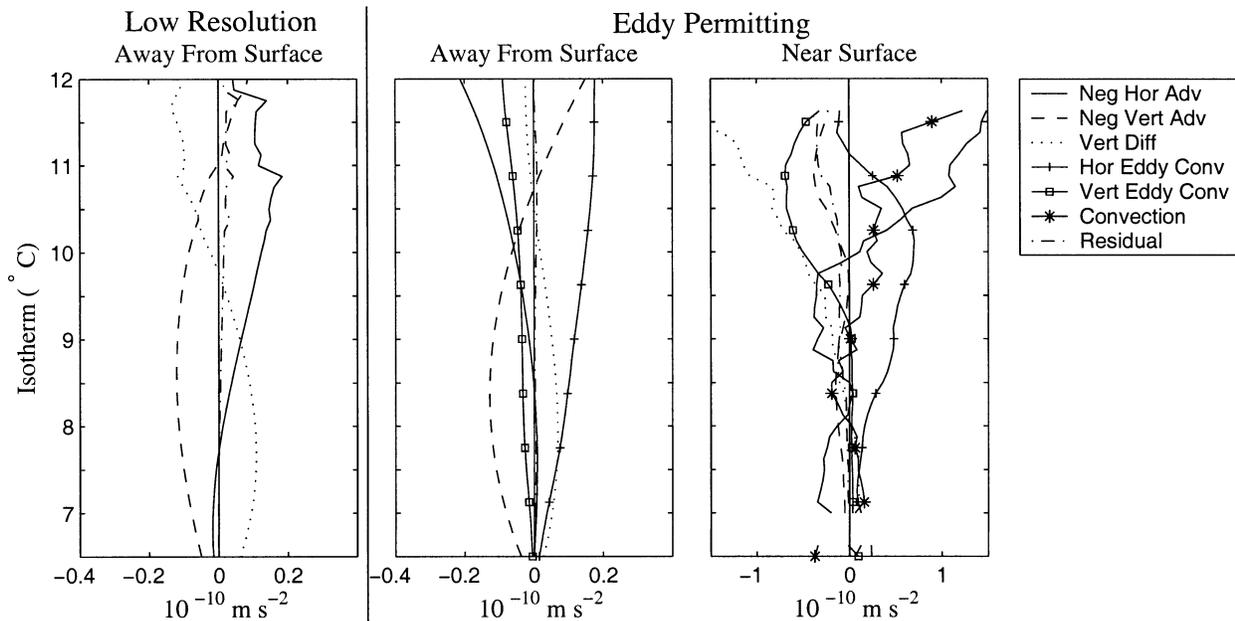
Internal Thermocline Buoyancy Terms

FIG. 12. As in Fig. 9, but averaged along the isotherms in the internal thermocline.
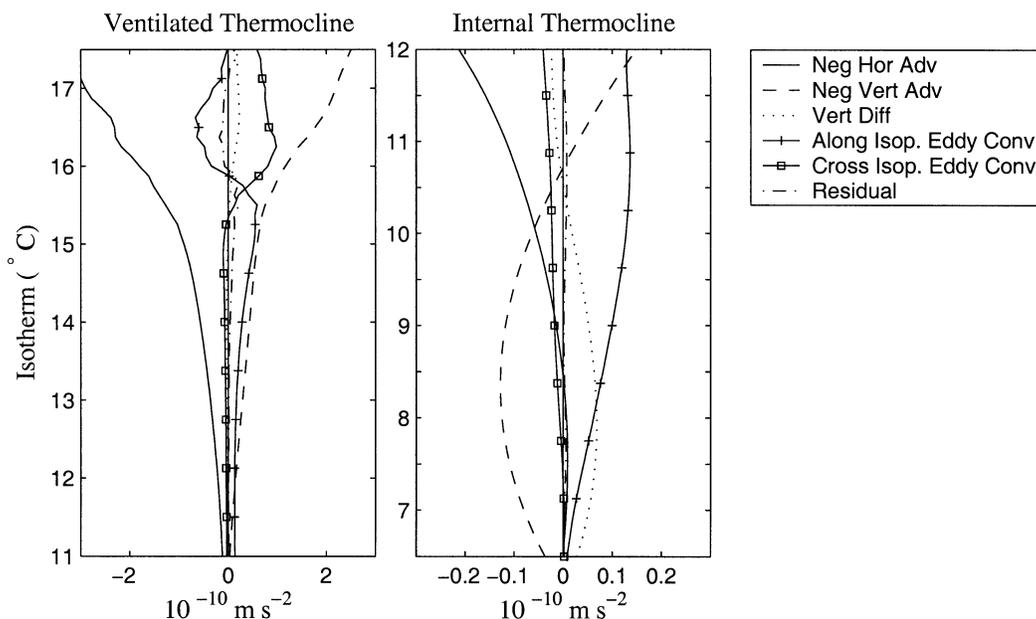
FIG. 13. The terms in the TEM form of the buoyancy equation, averaged along isotherms for the (left) ventilated thermocline and (right) internal thermocline. The along-isopycnal eddy flux convergence is $\mathbf{v}^* \cdot \nabla \overline{b}$, and the cross-isopycnal flux convergence is G_z. In regions where $\mathbf{v}^* \cdot \nabla \overline{b}$ is not zero, the eddies are inducing a cross-isopycnal mass flux.

the eddies have a strong barotropic component so that the amplitude of the eddies does not decay in the vertical as quickly as the amplitude of the mean flow.

The thickening of the internal thermocline by the eddy fluxes suggests that the eddies are effectively transferring thickness, or buoyant water mass, from the surface into the interior. From the right panel of Fig. 12, the poleward eddy fluxes are converging at the surface and creating a source of buoyancy. In steady state, this buoyancy is fluxed both to the atmosphere (identified as a negative diffusion term) and, by way of an eddy and mean flux, along isotherms into the interior (cf. Marshall 1997; Hazeleger and Drijfhout 2000). In the interior, the along-isopycnal eddy buoyancy fluxes are convergent, supplying mass to and thereby thickening the internal thermocline. We now diagnose this from a transformed Eulerian mean (TEM) perspective.

d. Residual circulation and the transformed Eulerian mean

Without approximation, the buoyancy equation in (3) can be written in the TEM form as

$$\frac{\partial b}{\partial t} + (\overline{\mathbf{v}} + \mathbf{v}^*) \cdot \nabla b = -G_z + \kappa_v b_{zz}, \quad (17)$$

where

$$\mathbf{v}^* = \left[-\left(\frac{\overline{u'b'}}{\overline{b}_z}\right)_z, \ -\left(\frac{\overline{v'b'}}{\overline{b}_z}\right)_z, \ \left(\frac{\overline{u'b'}}{\overline{b}_z}\right)_x + \left(\frac{\overline{v'b'}}{\overline{b}_z}\right)_y \right]$$

$$(18)$$

is a three-dimensional "eddy-induced velocity" and

$$G = \frac{\overline{\mathbf{v}'b'} \cdot \nabla \overline{b}}{\partial \overline{b}/\partial z}, \quad (19)$$

and the reader can verify that

$$G_z + \mathbf{v}^* \cdot \nabla b \equiv \nabla \cdot \overline{\mathbf{v}'b'} \quad (20)$$

(Andrews et al. 1987). This transformation separates the eddy flux convergence (nonuniquely) into the contributions from the along-isopycnal and cross-isopycnal eddy fluxes. The cross-isopycnal flux convergence is reexpressed as G_z, which accounts for the convergence of the explicitly diapycnal eddy buoyancy fluxes. The along-isopycnal flux convergence is reexpressed as advection by an eddy-induced, volume-conserving velocity, $\mathbf{v}^*$ (that is, $\nabla \cdot \mathbf{v}^* = 0$). When these along-isopycnal eddy fluxes have net convergence, or $\mathbf{v}^* \cdot \nabla \overline{b}$ is nonzero, then $\mathbf{v}^*$ has a component that crosses the mean isopycnals. Put another way, convergent along-isopycnal buoyancy fluxes can drive a cross-isopycnal mass flux.

Figure 13 shows the TEM form of the eddying buoyancy equation terms averaged along isotherms in the ventilated thermocline (left) and internal thermocline

(right). In the ventilated thermocline away from the surface, the eddy flux convergence is entirely due to the along-isopycnal fluxes and G_z is close to zero. Along isotherms 16–18, which lie within 50 m of the surface, G_z is large, again indicating that the eddies are explicitly cross-isopycnal and diabatic at the surface.

In the internal thermocline, where the buoyancy equation is a three-way balance between the mean vertical advection, eddy flux convergence, and vertical diffusion, we find that G_z is again small. Given this observation, the eddy convergence can be reexpressed as an eddy-induced cross-isopycnal advection,

$$(\overline{u'b'})_x + (\overline{v'b'})_y + (\overline{w'b'})_z = u^*\overline{b}_x + v^*\overline{b}_y + w^*\overline{b}_z. \tag{21}$$

An explicit diagnosis of the individual eddy advection terms reveals that $w^*\overline{b}_z$ dominates over $u^*\overline{b}_x + v^*\overline{b}_y$ (not shown), so that the eddy convergence terms can be approximated by $w^*\overline{b}_z$. The balance in the buoyancy equation becomes

$$(\overline{w} + w^*)b_z \approx \kappa_v b_{zz}. \tag{22}$$

The left-hand side of the above equation is the residual mean upwelling, w_{res}, through the base of the thermocline.

What would happen if the vertical diffusion were to go to zero? In this case $\mathbf{v}_{res} \cdot \nabla b$ must be zero and there would be no residual mean flow crossing isopycnals. However, unlike the low-resolution models, there seems to be a priori no requirement that the thickness of the internal thermocline need go to zero in this limit. The convergent eddy buoyancy fluxes, and their associated eddy-induced mass flux, would balance the mean upwelling. However, these convergent buoyancy fluxes could continue to mix buoyant water masses from the mixed layer into the internal thermocline, thickening the front even in the absence of explicit diffusion. We revisit this issue in section 5b.

e. Western boundary region

In contrast to the gyre portion, the eddies play a dominant role in setting the stratification in the western boundary current region. In the low-resolution case, a plot of the buoyancy equation terms reveals a balance between the mean advection terms and the horizontal diffusivity (not shown). If the horizontal diffusivity is reduced, the solution becomes unsteady. In the eddy-permitting case, the horizontal diffusion term is small, but it is replaced by a large-eddy convergence term. We must conclude that the eddies are important in setting the stratification within the western boundary region, and that for the low-resolution case the horizontal diffusivity is (perhaps unrealistically) substituting for their effects.

Figure 14 shows the depth of the 11° isotherm in the low-resolution and eddy-permitting cases. In the west-
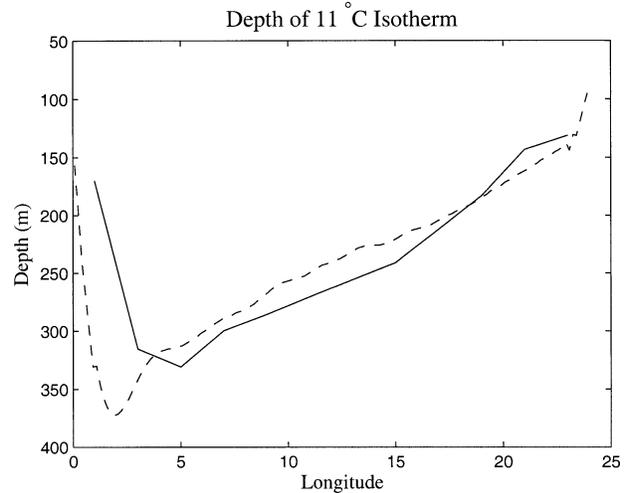

FIG. 14. The depth of the 11°C isotherm at 25°S. The low-resolution case is the solid line, and the eddy-permitting case is the dashed line. In the gyre, the depths are largely similar. However, within the western boundary region, the eddying case shows a steeper slope over a narrower region.

ern boundary region, the slope becomes steeper and the region as a whole becomes narrower. Clearly, the eddies are responsible for setting the slope of the isotherms in the western boundary region, and this slope changes when the eddies are explicitly included rather than parameterized. Further study is warranted but is beyond the scope of this paper.

5. Varying the winds and diffusivity

We now explore how the various properties of the thermocline, in particular its depth and thickness, vary with the strength of the wind and the diffusivity. Table 1 indicates the experiments performed: the base case provides a pivot around which we separately vary the wind and the diffusivity, integrating each experiment for more than 100 yr to ensure that a near-equilibrium is obtained.

a. Depth of the ventilated thermocline

In a noneddying model, the balance between the mean advection terms implies the depth of the ventilated thermocline should depend on the strength of the Ekman pumping to the half power, as given in (7). As described in Table 1, we ran the low-resolution and eddy-permitting experiments with a total of four different wind strengths. It is worth emphasizing that in our model, the changed parameter is the strength of the wind; this parameter then enters the scaling theory via the Ekman pumping. Figure 15 shows the depth of the thermocline as a function of downwelling strength on a log plot for both the low-resolution and eddy-permitting cases. The base case from our earlier analysis is given a normalized downwelling strength of 1. The low-resolution case,
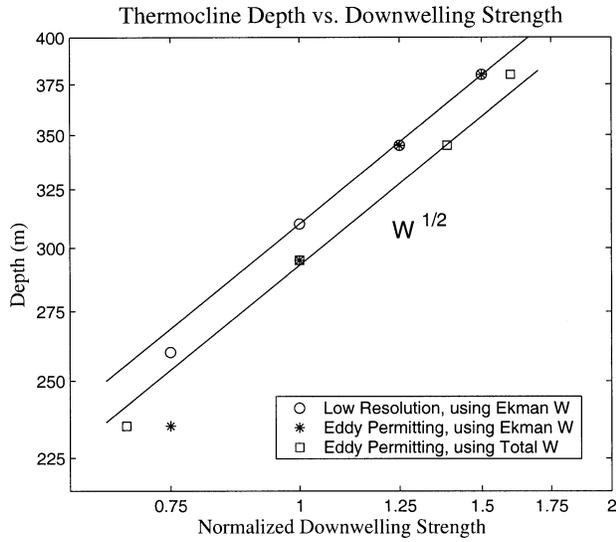
Thermocline Depth vs. Downwelling Strength

FIG. 15. A log–log plot of the depth of the ventilated thermocline as a function of the normalized downwelling strength for the low-resolution case (circles) and eddy-permitting case when plotted as a function of the Ekman pumping (stars) and the eddy-permitting case when plotted as a function of the total downwelling (squares). The base case analyzed in section 4 is the case with normalized downwelling of 1.

shown with circles in the figure, scales as the Ekman pumping (or wind strength) to the half power, consistent with an advective balance.

For the eddying cases, the stars show the depth of the thermocline as a function of the Ekman pumping strength (as inferred from the wind strength). These depths do not follow a dependence on the Ekman pumping to the half power, as a mean advection balance would suggest; the dependence is somewhat steeper for the low wind cases, although further analysis reveals a dominant balance between the mean advection terms in the buoyancy equation in all cases. This discrepancy suggests the difference arises from an eddy-induced change to the mean downwelling. The squares in the figure show the depths as a function of the explicit mean downwelling (as opposed to the Ekman pumping velocity), where we have calculated this value as the average downwelling within the diagnostics region at the uppermost grid box. These depths do support a dependence on the mean downwelling to the half power, consistent with the balance of terms in the buoyancy equation and the resulting scaling theory predictions. However, because the mean downwelling has changed, the eddies are affecting the thermocline depth indirectly. As we saw in section 4b(2), the eddies are diabatic at the surface and tend to shift the outcrop latitudes and affect the mean subduction from the mixed layer into the interior. This fact enters the scaling theory via the mean downwelling, and this eddy-induced change is small and is more dramatic for lower winds.

b. Internal thermocline thickness

In a noneddying model, the internal thermocline thickness scales as the diffusion to the half power:

$$\delta \sim \left(\frac{fL^2}{\Delta b W_e}\right)^{1/4} \kappa_v^{1/2}. \qquad (23)$$

When eddies are added, there is an eddy-induced downwelling in the region beneath the main ventilated thermocline where the eddy fluxes are convergent. Here, the diffusion must balance the residual mean vertical advection,

$$(\overline{w} + w^*)\overline{b}_z \approx \kappa_v \overline{b}_{zz}. \qquad (24)$$

We again assume that the fluxes mix down the mean buoyancy gradient with diffusivity κ_e, so that

$$\overline{v'b'} \approx -\kappa_e \overline{b}_y, \qquad (25)$$

where $\kappa_e \sim U_e L_e$. Then using (18) and assuming the x variations are smaller than the variations in y we have

$$\left[\overline{w} + \left(-\kappa_e \frac{\overline{b}_y}{\overline{b}_z}\right)_y\right]\overline{b}_z = [\overline{w} + (\kappa_e s)_y]\overline{b}_z \approx \kappa_v b_{zz}, \qquad (26)$$

where $s = -\overline{b}_y/\overline{b}_z$ is the slope of the isopycnals.

Let us assume that $U_e \sim CU$, where C is an $O(1)$ constant and U is the horizontal velocity scale and that $W \sim U\delta/L$, where δ is the thermocline thickness. This gives

$$\left(\frac{U\delta}{L} + Cs\frac{UL_e}{L}\right) \sim \frac{\kappa_v}{\delta}. \qquad (27)$$

Strictly speaking, this three-way balance cannot be used as a scaling theory, but it is instructive to examine several limits of this scaling. If the eddy fluxes (and so κ_e) are zero and using thermal wind balance

$$U \sim \frac{\Delta b \delta}{fL_i} \sim \frac{\Delta bD}{fL}, \qquad (28)$$

then (27) reduces to the classical diffusive scaling for the thermocline thickness (23). If instead $\kappa_v \to 0$ and the terms on the left-hand side remain finite and balance each other, then

$$\delta \sim sL_e. \qquad (29)$$

That is, the thickness of the internal thermocline is the product of its slope and the eddy scale, a seemingly sensible result. This suggests that the thickness of the thermocline might remain finite for small diffusivity, provided it has a finite slope that is independent of the value of the diffusivity (in order to provide baroclinic instability), and provided the eddy scale is nonzero. If the eddy scale is the deformation radius, $(\Delta bD)^{1/2}/f$, and noting that the slope of the isopycnals is given by D/L, where D is the depth of the ventilated thermocline (7), we obtain

$$\delta \sim \left(\frac{W_E^3 L^2}{\Delta b f} \right)^{1/4}. \tag{30}$$

A third balance is conceivable if the mean flow is weak and the eddies balance the explicit diffusion. In this case the slope of the isopycnals is determined by the nature of diabatic forcing at the surface, rather than the wind. The balance is then

$$s \frac{UL_e}{L} \sim \frac{\kappa}{\delta}. \tag{31}$$

If $s \sim (\delta/L)$, $U \sim \delta \Delta b/(fL)$ (by thermal wind) we obtain

$$\delta \sim \begin{cases} \left(\dfrac{\kappa f L^2}{\Delta b} \right)^{1/3} & \text{for } L_e = L \\[2ex] \left(\dfrac{\kappa^2 f^4 L^6}{\Delta b^3} \right)^{1/7} & \text{for } L_e = L_d = \dfrac{(\Delta b \delta)^{1/2}}{f}. \end{cases} \tag{32}$$

The first case is the classical diffusive scaling for the depth of the thermocline, and this arises because of the choice $L_e = L$. The second choice uses the deformation scale as the eddy scale. Other possibilities exist, but we do not explore this case further.

If eddies are present and the diffusion and mean flow remain important, as in our base case, then the model thermocline should lie between the two limits of (23) and (29) or (30). In this case, the thickness will have some dependence on the diffusivity, with the power law lying between $\kappa_v^{1/2}$ (no eddies) and diminishing dependence (no diffusion). However, we should note that this argument is very heuristic: no attempt has been made to actually solve the equations, and the structure of $\overline{w}$ and w^* may not support such a balance.

Figure 16 shows the thickness of the internal thermocline as a function of the normalized diffusivity for the low-resolution case (circles) and eddying case (stars). The low-resolution case indicates a dependence on the diffusivity to the half power. By comparison, the eddy-permitting thickness is thicker than the low-resolution counterpart for all diffusivities tested. This is consistent with the idea that the eddies are adding thickness by subducting buoyant water from the mixed layer into the internal thermocline. In this portion of parameter space, the dependence on the diffusivity remains close to, if somewhat shallower than, $\kappa_v^{1/2}$. Further investigation, probably with a model using isopycnal coordinates and very high vertical resolution, would be necessary to verify that the thickness remains finite as the diffusivity goes to zero.

6. Summary and discussion

In this paper, we have explored how the inclusion of mesoscale eddies affects the structure of the main thermocline. In a case without eddies, this thermocline has an upper, advective thermocline, a weakly stratified
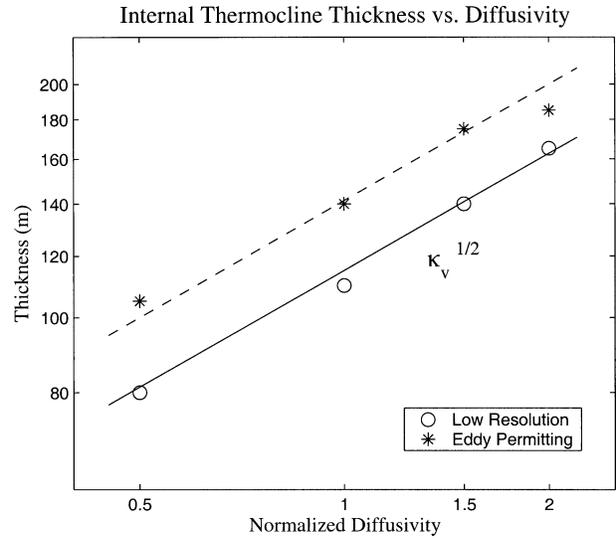

FIG. 16. A log–log plot of the thickness of the internal thermocline as a function of the normalized vertical diffusivity for the low-resolution case (circles) and eddy-permitting case (stars). The base case analyzed in section 4 is the case with normalized diffusivity of 1.

mode water region, and a lower diffusive region. We have examined how both the details of the stratification and the overall mean stratification change with the addition of eddies, and Fig. 17 summarizes our view of the main subtropical thermocline away from the western boundary current and in the presence of eddies.

We find that eddies have a quantitative and in some places qualitative effect on thermocline structure. A general conclusion is that eddies have a largely adiabatic effect in the ocean interior, away from the surface. That is to say, they do not directly transform water mass properties and their effects are, in principle, parameterizable by an advective term. However, near the surface their effects are clearly diabatic with decidedly across-isopycnal divergent buoyancy flux terms that noticeably affect outcrop latitudes.

Even though the model produces a vigorous mesoscale eddy field, we find that the dynamics of the model ventilated thermocline (away from the surface) remain dominated by the mean advective dynamics, with the eddy convergence terms being smaller than mean terms. Of course, this result is to some degree a function of how strong the eddies are in our numerical model, but they would have to be significantly and arguably unrealistically stronger (the eddy kinetic energy would have to be an order of magnitude larger) to qualitatively alter this balance. However, the eddies do tend to mix away the mode water region, which represents a storehouse of available potential energy in the low-resolution case. Indeed, the mode water is almost completely eroded away by the effects of eddies, suggesting that seasonal effects, not included in our simulations, may play a role in its maintenance in the real ocean. By changing the buoyancy equation balance in the mixed layer, ed-
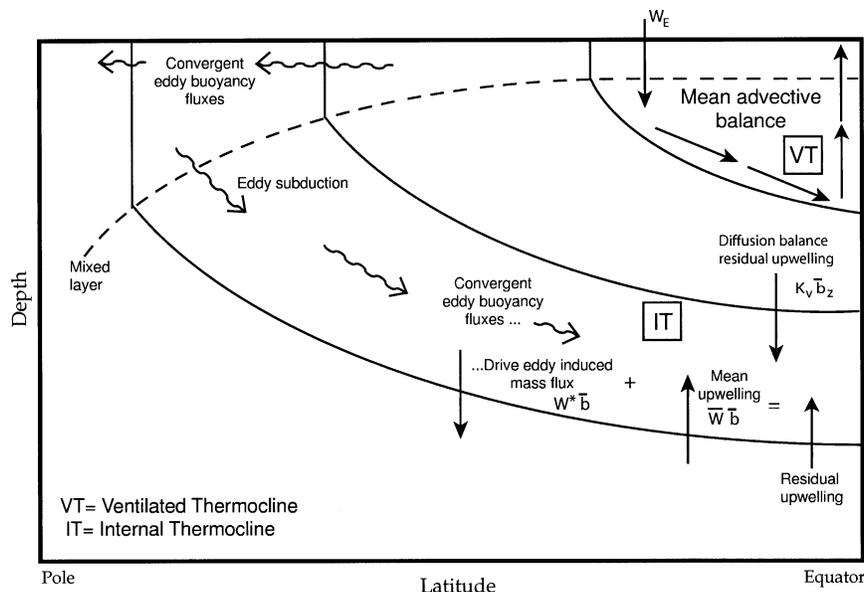
FIG. 17. A schematic of the thermocline in an eddying ocean. In the ventilated thermocline, the balance remains between the mean advection terms. At the surface in the subpolar gyre, convergent eddy fluxes drive eddy subduction into the internal thermocline. The warm surface water mass is spread along the isopycnals by convergent eddy fluxes, which drive an eddy-induced advection. This advection is balanced by the mean upwelling through the base of the thermocline, and residual upwelling must be balanced by the vertical diffusion.

dies also change the mean subduction rate of water into the ventilated thermocline. This enters the scaling theory via the mean downwelling, so that changes to the ventilated thermocline depth can be traced to the diabatic eddy effects at the surface. Still, overall, the depth of the ventilated thermocline continues to depend on the mean downwelling to the half power, as in classical noneddying theory.

The internal thermocline is, perhaps surprisingly, more affected by the presence of eddies than is the ventilated thermocline. This arises because the intensity of eddies decays more slowly with depth than does that of the mean flow. In the absence of eddies and in simple geometries the base of the ventilated thermocline is coincident with the level at which vertical velocity vanishes. This is an advective–diffusive region, which collapses to a front in the limit of zero diffusivity. The location of the front appears to be little altered by the presence of mesoscale eddies, but the dynamics of the front itself does change. Typically, the internal thermocline thickens: thickness created in the surface layer is effectively mixed along isopycnals by eddy fluxes, separating the isotherms of the internal thermocline and thickening the front. These eddy fluxes can be associated with an eddy-induced downwelling that partially balances the mean upwelling through the thermocline. Any net residual mean upwelling must then be balanced by the diffusion. In the case of vanishingly small diffusivity (which is difficult to reach in a z-coordinate model) the residual circulation would have to go to zero, but the mean thickness of the internal thermocline might remain

finite as the eddies continue to transfer buoyant water masses from the surface to the interior of the isopycnals. In this case potential vorticity within the internal thermocline might become homogenized so determining the thickness of the thermocline. Other possibilities and scalings are discussed in the text, but a definitive determination of the thickness of the internal thermocline in the presence of mesoscale eddies is beyond our current grasp.

Last, we remark that although eddies may not be responsible for setting the depth of the ventilated thermocline in midgyre, equilibration of the western boundary region does rely on the presence of eddies or a parameterization of their effects. Thus, for example, in the noneddying integrations the horizontal diffusivity unavoidably plays a role in the western boundary current dynamics. Such a picture is generally consistent with that of Radko and Marshall (2003) who find that on a β plane, the mass balance of the thermocline is dominated by eddy shedding, but this shedding occurs in the western boundary layer. As β increases eddies become less important in the gyre, the interior is Sverdrupian and the gyre region depth is given by the mean advective scaling.

In general, our results are robust across the parameter space explored in this paper, but that space is necessarily limited. At the surface, we have used a restoring scheme, with the restoring strength such that the heat fluxes in the western boundary region are the correct order of magnitude when compared with the real ocean. Based on the ideas of Huang (1989), Drijfhout (1994) sug-

gested that the eddy-induced modification of the surface outcrops will depend on the effective advection time scale of the eddies and the effective restoring time over the depth of the mixed layer. In our model, the restoring time is short in comparison with the eddy advection time, and the eddies can modify the surface outcrops and mixed-layer buoyancy balances. Thus, a change in restoring time scale would likely change the subduction rates out of the mixed layer and therefore change the internal thermocline thickness. This serves to emphasize the role of interactions between the mixed layer and mesoscale eddies, a worthy topic for further investigation.

REFERENCES

Andrews, D. G., J. R. Holton, and C. B. Levy, 1987: *Middle Atmosphere Dynamics.* Academic Press, 489 pp.

Chelton, D. B., R. A. deSzoeke, M. G. Schlax, K. E. Naggar, and N. Siwertz, 1998: Geographical variability of the first-baroclinic Rossby radius of deformation. *J. Phys. Oceanogr., 28,* 433–460.

Cox, M. D., 1985: An eddy resolving numerical-model of the ventilated thermocline. *J. Phys. Oceanogr., 15,* 1312–1324.

Drijfhout, S. S., 1994: Sensitivity of eddy-induced heat transport to diabatic forcing. *J. Geophys. Res., 99,* 18 481–18 499.

Gent, P. R., J. Willebrand, T. McDougall, and J. C. McWilliams, 1995: Parameterizing eddy-induced tracer transports in ocean circulation. *J. Phys. Oceanogr., 25,* 463–474.

Griffies, S. M., R. C. Pacanowski, and R. W. Hallberg, 2000: Spurious diapycnal mixing associated with advection in a *z*-coordinate ocean model. *Mon. Wea. Rev., 128,* 538–564.

Hazeleger, W., and S. S. Drijfhout, 2000: Eddy subduction in a model of the subtropical gyre. *J. Phys. Oceanogr., 30,* 677–695.

Huang, R. X., 1988: On boundary value problems of the ideal-fluid thermocline. *J. Phys. Oceanogr., 18,* 619–641.

——, 1989: Sensitivity of a multilayered oceanic general circulation model to the sea surface thermal boundary condition. *J. Geophys. Res., 94,* 18 011–18 021.

Kamenovich, I., J. Marotzke, and P. H. Stone, 2000: Factors affecting heat transport in an ocean general circulation model. *J. Phys. Oceanogr., 30,* 175–194.

Karsten, R., H. Jones, and J. Marshall, 2002: The rold of eddy transfer in setting the stratification and transport of a circumpolar current. *J. Phys. Oceanogr., 32,* 39–54.

Luyten, J. R., J. Pedlosky, and H. Stommel, 1983: The ventilated thermocline. *J. Phys. Oceanogr., 13,* 292–309.

Marshall, D. P., 1997: Subduction of water masses in an eddying ocean. *J. Mar. Res., 55* (2), 201–222.

Marshall, J., H. Jones, R. Karsten, and R. Wardle, 2002: Can eddies set ocean stratification? *J. Phys. Oceanogr., 32,* 26–38.

Nakamura, M., and Y. Chao, 2000: On the eddy isopycnal thickness diffusivity of the Gent–McWilliams subgrid mixing parameterization. *J. Climate, 13,* 502–510.

Oort, A. H., S. C. Ascher, S. Levitus, and J. P. Peixoto, 1989: New estimates of the available potential-energy in the World Ocean. *J. Geophys. Res., 94* (C3), 3187–3200.

Pacanowski, R. C., and S. M. Griffies, 1999: *The MOM-3 Manual, Alpha Version.* NOAA/Geophysical Fluid Dynamics Laboratory, 580 pp.

Radko, T., and J. Marshall, 2003: Equilibration of a warm pumped lens on a β plane. *J. Phys. Oceanogr., 33,* 885–899.

Rhines, P. B., 1975: Waves and turbulence on a beta-plane. *J. Fluid Mech., 69,* 417–443.

——, and W. R. Young, 1982: Homogenization of potential vorticity in planetary gyres. *J. Fluid Mech., 122,* 347–367.

Richardson, P. L., 1983: Eddy kinetic-energy in the North-Atlantic from surface drifters. *J. Geophys. Res., 88* (NC7), 4355–4367.

Robinson, A. R., and H. Stommel, 1959: The oceanic thermocline and the associated thermohaline circulation. *Tellus, 11,* 295–308.

Salmon, R., 1990: The thermocline as an internal boundary layer. *J. Mar. Res., 44,* 695–711.

Samelson, R. M., 1999: Internal boundary layer scaling in "two-layer" solutions of the thermocline equations. *J. Phys. Oceanogr., 29,* 2099–2102.

——, and G. K. Vallis, 1997: Large-scale circulation with small diapycnal diffusion: The two-thermocline limit. *J. Mar. Res., 55,* 223–275.

Smith, K. S., and G. K. Vallis, 2002: The scales and equilibration of midocean eddies: Forced-dissipative flow. *J. Phys. Oceanogr., 32,* 1699–1721.

Stammer, D., 1997: Global characteristics of ocean variability estimated from regional TOPEX/Poseidon altimeter measurements. *J. Phys. Oceanogr., 27,* 1743–1769.

Stommel, H., and J. Webster, 1963: Some properties of the thermocline equations in a subtropical gyre. *J. Mar. Res., 44,* 695–711.

Vallis, G. K., 2000: Thermocline theories and WOCE: A mutual challenge. *International WOCE Newsletter*, No. 39, WOCE International Project Office, Southampton, United Kingdom, 3–5.

——, and M. E. Maltrud, 1993: Generation of mean flows and jets on a beta plane and over topography. *J. Phys. Oceanogr., 23,* 1346–1362.

Veronis, G., 1975: The role of models in tracer studies. *Numerical Models of the Ocean Circulation,* National Academy of Sciences, 133–146.

Welander, P., 1959: An advective model of the ocean thermocline. *Tellus, 11,* 309–318.

Wyrtki, K., L. Magaard, and J. Hager, 1976: Eddy energy in oceans. *J. Geophys. Res., 81,* 2641–2646.